

Advection of Inertial Particles in the Presence of the History Force: Higher Order Numerical Schemes

Anton Daitche

Institute for Theoretical Physics, Westfälische Wilhelms-Universität, Wilhelm-Klemm-Str. 9, D-48149 Münster, Germany

Abstract

The equations describing the motion of finite-size particles (inertial particles) contain in their full form the history force. This force is represented by an integral whose accurate numerical evaluation is rather difficult. Here, a systematic way is presented to derive numerical integration schemes of arbitrary order for the advection of inertial particles with the history force. This involves the numerical evaluation of integrals with singular, but integrable, integrands. Explicit specifications of first, second and third order schemes are given and the accuracy and order of the schemes are verified using known analytical solutions.

Keywords: history force, inertial particles, numerical approximation, Maxey-Riley equation, fractional differential equation, singular integrand

The advection of finite-size particles (often called inertial particles) plays an important role in engineering [1] and in many environment-related phenomena ranging from meteorology to oceanography, e.g. cloud microphysics [2]. Particle-based modeling has been applied to the formation of planetesimals in the early solar system [3] and the aggregation and fragmentation processes in fluid flows [4]. Example applications are pollutant-transport forecasting for homeland defense [5], and the location of a toxin or biological pathogen spill (e.g. anthrax) from outbreaks in a street canyon [6]. Other recent results indicate that inertial particles might play a role in hurricane dynamics [7] and in the feeding dynamics of certain marine animals [8].

The basic equation of motion for a small spherical particle of radius a and mass m_p in a viscous fluid is given by the Maxey-Riley equation [9, 10]:

$$m_p \frac{d\mathbf{v}}{dt} = m_f \frac{D\mathbf{u}}{Dt} - \frac{m_f}{2} \left(\frac{d\mathbf{v}}{dt} - \frac{D\mathbf{u}}{Dt} \right) - 6\pi a \varrho_f \nu (\mathbf{v} - \mathbf{u}) - 6a^2 \varrho_f \sqrt{\pi \nu} \int_{t_0}^t \frac{1}{\sqrt{t-\tau}} \left(\frac{d\mathbf{v}}{d\tau} - \frac{d\mathbf{u}}{d\tau} \right) d\tau. \quad (1)$$

Here, $\mathbf{v} = d\mathbf{r}/dt$ is the particle velocity, $\mathbf{u}(\mathbf{r}, t)$ the fluid velocity, m_f the mass of the fluid excluded by the particle, ν the kinematic viscosity of the fluid and ϱ_f the density of the fluid. The two appearing derivatives

$$\frac{d\mathbf{u}}{dt} = \frac{\partial \mathbf{u}}{\partial t} + \mathbf{v} \cdot \nabla \mathbf{u} \quad \text{and} \quad \frac{D\mathbf{u}}{Dt} = \frac{\partial \mathbf{u}}{\partial t} + \mathbf{u} \cdot \nabla \mathbf{u}$$

denote the full derivative along the trajectory of the particle and of the corresponding fluid element, respectively. The terms on the right-hand side of (1) are: the force exerted by the fluid on a fluid element at the location of the particle, the added mass term describing the impulsive pressure response of the fluid, the Stokes drag, and the history force. In this form of the equation, gravity and the so-called Faxén corrections are not included. The history force accounts for the viscous diffusion of vorticity from the surface of the particle along its trajectory [9] and renders the advection equation to be an integro-differential equation whose solution is much more demanding than that of an ordinary differential equation. Because of this difficulty, this integral term is neglected in nearly all the applications mentioned above. However, experimental and analytic efforts [11, 12] indicate that the history force might have significant effects for non-neutrally-buoyant

Email address: anton.d@wwu.de (Anton Daitche)

particles in simple flows. Recent studies have also shown that the history force is relevant in turbulent flows [13, 14] and chaotic advection [15]. The present paper will detail the derivation and analysis of the numerical schemes developed for the investigations in the latter study.

An important condition for the validity of equation (1) is that the particle Reynolds number $Re_p = |\mathbf{v} - \mathbf{u}|a/\nu$ remains small during the entire dynamics [9]. Furthermore the particle's size a and its diffusive time scale $\tau_\nu = a^2/\nu$ have to be (much) smaller than the smallest length and time scales of the flow, respectively. For particles of comparable size as the smallest length scale so-called Faxén corrections will become important [9]. Several attempts [16, 17, 18] have been made to extend (1) to the case of finite particle Reynolds numbers by modifying the particular form of the forces. Part of all of these approaches is a different form of the history force. The numerical schemes presented here can be applied to these forms as well (with some minor modifications) as will be discussed in section 5. Note also that besides the history force, further modifications of (1) can be necessary for finite particle Reynolds numbers, e.g. non-linear drag and the so-called lift force (see [19] for a review).

The history force poses the main difficulty for a numerical integration of (1). There are basically three problems: (i) the singularity of the kernel $1/\sqrt{t-\tau}$, (ii) the fact that (1) is an implicit integro-differential equation due to the appearance of $d\mathbf{v}/dt$ on the right-hand side and (iii) the high computational costs for a numerical integration. The first point (i) is the most involved one and will be addressed by a special quadrature¹ scheme. The implicitness (ii) is not a major issue and can be addressed rather easily as we will see. The last point (iii) stems from the necessity to recompute the history force – an integral over all previous time-steps – for every new time-step. Therefore the computational costs grow with the square of the the number of time-steps and can become quite substantial for long integration periods. This difficulty is inherent to the dynamics governed by the history force and cannot be addressed without further approximations. Note however that a higher order scheme reduces the number of necessary time-steps and therefore diminishes the problem of high computational costs indirectly. Furthermore the final form of the numerical scheme will be formulated as a weighed sum, which is well suited for a numerical evaluation on modern CPU architectures.

The correct numerical treatment of the full Maxey-Riley equation and in particular of the history force has received little interest in the past, in spite of an increasing number of studies supporting its importance. Michaelides [20] transformed the Maxey-Riley equation to a second order equation in which the history integral contains only the fluid velocity, but not the particle velocity. This makes the evolution equation explicit. Furthermore, according to Michaelides, this form of the equation allows a sparser sampling of the particle's history, which leads to savings in computational time and computer memory. However, the history integral still has a similar form as in (1) and the difficulties of an accurate numerical evaluation remain. Two previously proposed schemes addressing the history integral have been tested by Bombardelli et al. [21]. They found the accuracy of the schemes to be $\mathcal{O}(\sqrt{h})$ and $\mathcal{O}(h)$, where h is the time-step. In a recent work Hinsberg et al. [22] have proposed a first order² scheme for the computation of the history force, i.e. the error is $\mathcal{O}(h^2)$, which represents a significant advancement over previously known schemes. Furthermore Hinsberg et al. developed a method to decrease the needed amount of history for the computation of the history force, by approximating the tail of the history kernel with exponential functions. This leads to significant savings of computational time and computer memory. This method can be viewed as a major improvement over the method of a window kernel where the kernel is set to zero for time lags larger than a certain window time [18, 21].

The present paper will describe the construction of arbitrary high order methods for the integration of particle trajectories with the history force and will give explicit specification of the first, second and third order methods with an accuracy of $\mathcal{O}(h^2)$, $\mathcal{O}(h^3)$ and $\mathcal{O}(h^4)$, respectively. Approximate forms of the history kernel as mentioned above will not be considered. However, the developed schemes can be easily adapted to the window kernel or the more advanced approach proposed by Hinsberg et al.

¹In this article the term “quadrature scheme” refers to a numerical scheme for the approximation of an integral whereas the term “integration scheme” refers to a scheme for the approximation of the solution of the whole integro-differential equation.

²In the paper by Hinsberg et al. the scheme is said to be of second order. This is due to a different definition of the meaning of “order”. Here, a scheme with an error term proportional to the square of the time-step is considered to be of first order as it is accurate up to the first order; in the same sense as the Euler-method is a first order scheme.

The rest of the paper is structured as follows: First some general notes about the history force and the Maxey-Riley equation will be given. Afterwards a numerical quadrature scheme for the history force and its derivation will be presented. In the following section this quadrature scheme will be incorporated into an integration scheme for the numerical solution of the full Maxey-Riley equation. The full integration scheme will then be tested against known analytical solutions. This is followed by a section on the stability properties of the algorithm, and by a discussion and conclusion.

1. Introductory Notes

Measuring time and velocity in units of T and U , the dimensionless Maxey-Riley equation becomes

$$\frac{1}{R} \frac{d\mathbf{v}}{dt} = \frac{D\mathbf{u}}{Dt} - \frac{1}{S} (\mathbf{v} - \mathbf{u}) - \sqrt{\frac{3}{\pi}} \frac{1}{S} \int_{t_0}^t \frac{1}{\sqrt{t-\tau}} \left(\frac{d\mathbf{v}}{d\tau} - \frac{d\mathbf{u}}{d\tau} \right) d\tau. \quad (2)$$

Here two dimensionless parameters appear, the density parameter³

$$R = \frac{3m_f}{m_f + 2m_p},$$

and a ratio of the particle's viscous relaxation time and the characteristic time of the flow T

$$S = \frac{1}{3} \frac{a^2/\nu}{T}.$$

In smooth large-scale flows there is often only one typical time scale whereas in a turbulent flow there are many. In the latter case the smallest time scale, the Kolmogorov time τ_η , is appropriate.

Many of the derivations and concepts in this article are applicable for any kernel appearing in the history force integral. Therefore, in the following, a general kernel $K(t - \tau)$ will be used where the derivations do not depend on its particular form. The explicit specification of the quadrature scheme and the tests of the numerical schemes will be given for the standard kernel

$$K(t - \tau) = \frac{1}{\sqrt{t - \tau}}. \quad (3)$$

Before we proceed with the derivation of the quadrature scheme, let us first rewrite the history force integral in a different form

$$\int_{t_0}^t K(t - \tau) \frac{d}{d\tau} f(\tau) d\tau + K(t - t_0) f(t_0) = \frac{d}{dt} \int_{t_0}^t K(t - \tau) f(\tau) d\tau, \quad (4)$$

where $f(\tau) = \mathbf{v} - \mathbf{u}$. This relation can be verified using integration by parts⁴. Equation (1) has been derived with the assumption of a particle starting with the same initial velocity as the fluid, i.e. $\mathbf{v}(t_0) = \mathbf{u}(t_0)$. In this case the second term on the left-hand side of (4) vanishes. In the case of different initial velocity the additional term $(\mathbf{u}(t_0) - \mathbf{v}(t_0))/\sqrt{t - t_0}$ has been given in [20, 23], which is exactly the additional term appearing in (4). Therefore the Maxey-Riley equation can be written in the following form, which is now also valid for initial conditions with $\mathbf{v}(t_0) \neq \mathbf{u}(t_0)$,

$$\frac{1}{R} \frac{d\mathbf{v}}{dt} = \frac{D\mathbf{u}}{Dt} - \frac{1}{S} (\mathbf{v} - \mathbf{u}) - \sqrt{\frac{3}{\pi}} \frac{1}{S} \frac{d}{dt} \int_{t_0}^t d\tau K(t - \tau) (\mathbf{v} - \mathbf{u}). \quad (5)$$

³In some cases the density parameter is defined as $R = 2m_f/(m_f + 2m_p)$, which differs by a factor of 3/2 from the definition here.

⁴When the kernel has singularities, one has first to use integrals with the upper bound of $t - \epsilon$, then perform integration by parts and finally take the limit $\epsilon \rightarrow 0$ (to prevent the appearance of singularities outside of integrals). An alternative for the standard kernel is to use a transformation of the integration variable $\tau \rightarrow x = \sqrt{t - \tau}$.

It is beneficial to use this form of the history force because it enables us to compute an integral of the history force by simply dropping the derivative. This improves and simplifies the numerical scheme as we will see.

At this point it is interesting to note that for the standard kernel the history force is equal to a fractional derivative of the Riemann-Liouville type:

$$\left(\frac{d}{dt}\right)^{1/2} f(t) \equiv \frac{1}{\sqrt{\pi}} \frac{d}{dt} \int_{t_0}^t \frac{1}{\sqrt{t-\tau}} f(\tau) d\tau.$$

Thus the numerical methods developed here can be also considered as higher order methods for the numerical computation of fractional derivatives and the solution of fractional differential equations.

2. The Quadrature Scheme

In this section a systematic way is presented for the construction of quadrature schemes for integrals of the type

$$\int_{t_0}^t K(t-\tau) f(\tau) d\tau.$$

When the kernel K is a well behaved function no special effort is needed and standard schemes can be used. However in cases where the kernel has an integrable singularity, like e.g. the standard kernel (3) at $\tau = t$, standard numerical methods, like the Newton-Cotes⁵ schemes, lead to large errors as we will see. This is due to the necessity to evaluate the whole integrand including the kernel near the singularity. We will avoid this by constructing a specialized scheme in which the kernel is already integrated analytically.

Due to the linearity of the history integral with respect to f any quadrature scheme for this term can be expressed as a weighted sum

$$\int_{t_0}^t K(t-\tau) f(\tau) d\tau \approx \sum_{j=0}^n \mu_j f(\tau_j),$$

where $\tau_i = t_0 + hi$, $n = (t - t_0)/h$ and h is the time-step. The main topic of this section is the derivation and specification of the coefficients μ_j . The general procedure is to first split the integral into intervals of length h

$$\int_{t_0}^t K(t-\tau) f(\tau) d\tau = \sum_{i=0}^{n-1} \int_{\tau_i}^{\tau_{i+1}} K(t-\tau) f(\tau) d\tau,$$

then to approximate $f(\tau)$ in every of the intervals with a polynomial and finally to compute the appearing integrals analytically. The order of the polynomial will determine the order of the scheme.

Let us first examine the simplest case: a linear approximation leading to an order one scheme. By approximating⁶ $f(\tau)$ linearly in the interval $[\tau_i, \tau_{i+1}]$

$$f(\tau) = f(\tau_i) + \frac{f(\tau_{i+1}) - f(\tau_i)}{h} (\tau - \tau_i) + \mathcal{O}(h^2) \quad (6)$$

we obtain

$$\int_{\tau_i}^{\tau_{i+1}} K(t-\tau) f(\tau) d\tau = (f(\tau_i) + \mathcal{O}(h^2)) \int_0^h K(t-\tau_i-\tau) d\tau + \frac{f(\tau_{i+1}) - f(\tau_i)}{h} \int_0^h \tau K(t-\tau_i-\tau) d\tau.$$

In many cases the appearing integrals can be computed analytically, e.g. for the standard kernel (3)

$$\int_{\tau_i}^{\tau_{i+1}} \frac{f(\tau)}{\sqrt{t-\tau}} d\tau = (f(\tau_i) + \mathcal{O}(h^2)) \left[-2\sqrt{t-\tau_i-\tau}\right]_0^h + \frac{f(\tau_{i+1}) - f(\tau_i)}{h} \left[-2\tau\sqrt{t-\tau_i-\tau} - \frac{4}{3}(t-\tau_i-\tau)^{\frac{3}{2}}\right]_0^h.$$

⁵Well known Newton-Cotes schemes are e.g. the trapezoidal rule and Simpson's rule.

⁶The error of an approximation will be denoted by $\mathcal{O}(h^m)$, i.e. the error is bounded by Ch^m for some fixed C .

Summing up the terms for each of the intervals we obtain a formula for the whole integral, e.g. for the standard kernel

$$\int_{t_0}^t \frac{f(\tau)}{\sqrt{t-\tau}} d\tau = 2f(t_0)\sqrt{t-t_0} + \frac{4}{3} \sum_{i=0}^{n-1} \frac{f(\tau_{i+1}) - f(\tau_i)}{h} \left((t-\tau_i)^{\frac{3}{2}} - (t-\tau_{i+1})^{\frac{3}{2}} \right) + \mathcal{O}(h^2)\sqrt{t-t_0}. \quad (7)$$

Note that no singular or diverging expressions appear. For this it is crucial to approximate only $f(\tau)$ with polynomials, but not the whole integrand.

As already mentioned the quadrature scheme is linear in f and can thus be expressed as a weighted sum. Such a form is best suited for a numerical evaluation as modern processors/compiler can optimize this kind of operations rather well. We will index the coefficients of the sum in reversed order, i.e. we use the sum $\sum_j \mu_j f(\tau_{n-j})$ instead of $\sum_j \mu_j f(\tau_j)$. This is more natural as it turns out that the coefficient of $f(\tau_j)$ depends on $n-j$. For the standard kernel the coefficients for the first order quadrature scheme can be obtained from (7):

$$\int_{t_0}^t \frac{f(\tau)}{\sqrt{t-\tau}} d\tau = \sqrt{h} \sum_{j=0}^n \alpha_j^n f(\tau_{n-j}) + \mathcal{O}(h^2)\sqrt{t-t_0} \quad (8)$$

$$\alpha_j^n = \frac{4}{3} \begin{cases} 1 & j=0 \\ (j-1)^{3/2} + (j+1)^{3/2} - 2j^{3/2} & 0 < j < n \\ (n-1)^{3/2} - n^{3/2} + \frac{6}{4}\sqrt{n} & j=n. \end{cases} \quad (9)$$

Here the factor \sqrt{h} has been pulled out of the coefficients to make them independent of the time-step h . Also, note that the coefficients α_j^n depend on n , the number of intervals for the approximation of the integral. The first order scheme specified by (8) and (9) is equivalent to the one presented in [22], although the equivalence is not obvious.

The procedure just shown can be generalized to derive quadrature schemes of arbitrary high order. The basic ideas stay the same, however the technical details make the derivation complicated. Here, only a simplified overview of the construction will be given. The full derivation with all the technical details can be found in Appendix A.

To obtain a quadrature scheme of order m , we approximate f in every interval $[\tau_i, \tau_{i+1}]$ with an m -th order polynomial and solve the remaining integrals analytically. An interpolating polynomial of order m is uniquely determined by the values of f at $m+1$ time-points. Let us denote these time-points by θ_{ik} , where i is the index of the interval and $k \in \{0, \dots, m\}$. Using the Lagrangian representation of polynomial interpolation we obtain the approximation in the i -th interval

$$f(\tau) = \sum_{k=0}^m f(\theta_{ik}) L_{ik}(\tau) + \mathcal{O}(h^{m+1}) \quad L_{ik}(\tau) = \prod_{\substack{l=0 \\ l \neq k}}^m \frac{\tau - \theta_{il}}{\theta_{ik} - \theta_{il}}.$$

The time-points θ_{ik} can in principle be chosen arbitrary. However, it is clear that this choice will strongly influence the quality of the interpolation. Obviously, the points τ_i and τ_{i+1} should be included when interpolating in $[\tau_i, \tau_{i+1}]$. These time-points were our choice for the first order approximation (6). For higher order approximations we need more points additionally to τ_i and τ_{i+1} . Reasonable choices are the points closest to the bounds of the interval, i.e. $\tau_{i-1}, \tau_{i+2}, \tau_{i-2}, \dots$ (given we want to stay on the grid defined by the τ_i). And indeed we will use $\tau_{i-1}, \tau_i, \tau_{i+1}$ for the second order approximation and $\tau_{i-1}, \tau_i, \tau_{i+1}, \tau_{i+2}$ for the third order approximation. This can be generalized to arbitrary orders by choosing $\theta_{ik} = \tau_{i-\lfloor m/2 \rfloor + k}$ where the operation $\lfloor \cdot \rfloor$ denotes taking the integer part, often called the floor function.

With this definitions we can express the history integral as

$$\int_{t_0}^t d\tau K(t-\tau) f(\tau) = \sum_{i=0}^{n-1} \sum_{k=0}^m f(\theta_{ik}) \underbrace{\int_{\tau_i}^{\tau_{i+1}} d\tau K(t-\tau) L_k(\tau)}_{\lambda_{ik}} + E = \sum_{i=0}^{n-1} \sum_{k=0}^m f(\theta_{ik}) \lambda_{ik} + E,$$

where $E = \int_{t_0}^t K(t-\tau) d\tau \mathcal{O}(h^{m+1})$ is the error term. We naturally obtain a weighted double-sum due to the use of the Lagrangian representation of the interpolating polynomial, where the $f(\theta_{ik})$ appear as coefficients of the polynomials L_{ik} . Compare this with derivation of the first order scheme where we started from the linear interpolation (6), which is not in the Lagrangian form and thus a reordering of terms was necessary to get from (7) to (9).

The integrals λ_{ik} do not involve $f(\tau)$ and can be computed in advance; for many kernels even analytically, including the standard kernel. Now the final step is to reorder the double sum to a single weighted sum

$$\int_{t_0}^t d\tau K(t-\tau) f(\tau) = \sum_{i=0}^{n-1} \sum_{k=0}^m f(\theta_{ik}) \lambda_{ik} = \sum_{j=0}^n \mu_j^n f(\tau_{n-j}).$$

This procedure is detailed in Appendix A. Note that the coefficients μ_j^n (just like α_j^n) have a dependence on n .

In the following the coefficients for the standard kernel (3) will be given for a second and third order schemes, denoted by β_j^n and γ_j^n respectively. The factor \sqrt{h} has been extracted from the coefficients so that they do not depend on the time-step h .

The second order approximation is

$$\int_{t_0}^t d\tau \frac{1}{\sqrt{t-\tau}} f(\tau) = \sqrt{h} \sum_{j=0}^n \beta_j^n f(\tau_{n-j}) + \mathcal{O}(h^3) \sqrt{t-t_0} \quad (10)$$

with β_j^n for $n = 2$ and $n = 3$

$$\begin{aligned} \beta_{j=0,1,2}^2 &= \frac{12}{15} \sqrt{2}; \frac{16}{15} \sqrt{2}; \frac{2}{15} \sqrt{2} \\ \beta_{j=0,1,2,3}^3 &= \frac{4}{5} \sqrt{2}; \frac{14}{5} \sqrt{3} - \frac{12}{5} \sqrt{2}; -\frac{8}{5} \sqrt{3} + \frac{12}{5} \sqrt{2}; \frac{4}{5} \sqrt{3} - \frac{4}{5} \sqrt{2} \end{aligned}$$

and for $n \geq 4$

$$\beta_j^n = \begin{cases} \frac{4}{5} \sqrt{2} & j = 0 \\ \frac{14}{5} \sqrt{3} - \frac{12}{5} \sqrt{2} & j = 1 \\ \frac{176}{15} - \frac{42}{5} \sqrt{3} + \frac{12}{5} \sqrt{2} & j = 2 \\ \frac{8}{15} \left((j+2)^{5/2} - 3(j+1)^{5/2} + 3j^{5/2} - (j-1)^{5/2} \right) & 2 < j < n-1 \\ + \frac{2}{3} \left(-(j+2)^{3/2} + 3(j+1)^{3/2} - 3j^{3/2} + (j-1)^{3/2} \right) & \\ \frac{8}{15} \left(-2n^{5/2} + 3(n-1)^{5/2} - (n-2)^{5/2} \right) & j = n-1 \\ + \frac{2}{3} \left(4n^{3/2} - 3(n-1)^{3/2} + (n-2)^{3/2} \right) & \\ \frac{8}{15} \left(n^{5/2} - (n-1)^{5/2} \right) + \frac{2}{3} \left(-3n^{3/2} + (n-1)^{3/2} \right) + 2\sqrt{n} & j = n. \end{cases}$$

The third order approximation is

$$\int_{t_0}^t d\tau \frac{1}{\sqrt{t-\tau}} f(\tau) = \sqrt{h} \sum_{j=0}^n \gamma_j^n f(\tau_{n-j}) + \mathcal{O}(h^4) \sqrt{t-t_0} \quad (11)$$

with γ_j^n for $3 \leq n \leq 6$

$$\begin{aligned}
\gamma_{j=0..3}^3 &= \frac{68}{105}\sqrt{3}; \frac{6}{7}\sqrt{3}; \frac{12}{35}\sqrt{3}; \frac{16}{105}\sqrt{3} \\
\gamma_{j=0..4}^4 &= \frac{244}{315}\sqrt{2}; \frac{1888}{315} - \frac{976}{315}\sqrt{2}; -\frac{656}{105} + \frac{488}{105}\sqrt{2}; \frac{544}{105} - \frac{976}{315}\sqrt{2}; -\frac{292}{315} + \frac{244}{315}\sqrt{2} \\
\gamma_{j=0..5}^5 &= \frac{244}{315}\sqrt{2}; \frac{362}{105}\sqrt{3} - \frac{976}{315}\sqrt{2}; \frac{500}{63}\sqrt{5} - \frac{1448}{105}\sqrt{3} + \frac{488}{105}\sqrt{2}; -\frac{290}{21}\sqrt{5} + \frac{724}{35}\sqrt{3} - \frac{976}{315}\sqrt{2}; \\
&\quad \frac{220}{21}\sqrt{5} - \frac{1448}{105}\sqrt{3} + \frac{244}{315}\sqrt{2}; -\frac{164}{63}\sqrt{5} + \frac{362}{105}\sqrt{3} \\
\gamma_{j=0..6}^6 &= \frac{244}{315}\sqrt{2}; \frac{362}{105}\sqrt{3} - \frac{976}{315}\sqrt{2}; \frac{5584}{315} - \frac{1448}{105}\sqrt{3} + \frac{488}{105}\sqrt{2}; \frac{344}{21}\sqrt{6} - \frac{22336}{315} + \frac{724}{35}\sqrt{3} - \frac{976}{315}\sqrt{2}; \\
&\quad -\frac{1188}{35}\sqrt{6} + \frac{11168}{105} - \frac{1448}{105}\sqrt{3} + \frac{244}{315}\sqrt{2}; \frac{936}{35}\sqrt{6} - \frac{22336}{315} + \frac{362}{105}\sqrt{3}; -\frac{754}{105}\sqrt{6} + \frac{5584}{315}
\end{aligned}$$

and for $n \geq 7$

$$\gamma_j^n = \begin{cases} \frac{244}{315}\sqrt{2} & j = 0 \\ \frac{362}{105}\sqrt{3} - \frac{976}{315}\sqrt{2} & j = 1 \\ \frac{5584}{315} - \frac{1448}{105}\sqrt{3} + \frac{488}{105}\sqrt{2} & j = 2 \\ \frac{1130}{63}\sqrt{5} - \frac{22336}{315} + \frac{724}{35}\sqrt{3} - \frac{976}{315}\sqrt{2} & j = 3 \\ \frac{16}{105} \left((j+2)^{7/2} + (j-2)^{7/2} - 4(j+1)^{7/2} - 4(j-1)^{7/2} + 6j^{7/2} \right) \\ + \frac{2}{9} \left(4(j+1)^{3/2} + 4(j-1)^{3/2} - (j+2)^{3/2} - (j-2)^{3/2} - 6j^{3/2} \right) & 3 < j < n-3 \\ \frac{16}{105} \left(n^{7/2} - 4(n-2)^{7/2} + 6(n-3)^{7/2} - 4(n-4)^{7/2} + (n-5)^{7/2} \right) - \frac{8}{15}n^{5/2} \\ + \frac{4}{9}n^{3/2} + \frac{8}{9}(n-2)^{3/2} - \frac{4}{3}(n-3)^{3/2} + \frac{8}{9}(n-4)^{3/2} - \frac{2}{9}(n-5)^{3/2} & j = n-3 \\ \frac{16}{105} \left((n-4)^{7/2} - 4(n-3)^{7/2} + 6(n-2)^{7/2} - 3n^{7/2} \right) + \frac{32}{15}n^{5/2} \\ - 2n^{3/2} - \frac{4}{3}(n-2)^{3/2} + \frac{8}{9}(n-3)^{3/2} - \frac{2}{9}(n-4)^{3/2} & j = n-2 \\ \frac{16}{105} \left(3n^{7/2} - 4(n-2)^{7/2} + (n-3)^{7/2} \right) - \frac{8}{3}n^{5/2} + 4n^{3/2} + \frac{8}{9}(n-2)^{3/2} - \frac{2}{9}(n-3)^{3/2} & j = n-1 \\ \frac{16}{105} \left((n-2)^{7/2} - n^{7/2} \right) + \frac{16}{15}n^{5/2} - \frac{22}{9}n^{3/2} - \frac{2}{9}(n-2)^{3/2} + 2\sqrt{n} & j = n. \end{cases}$$

Now that the quadrature schemes are fully specified, let us verify the correctness of the derivation and in particular the order of the schemes by using a test-case where the analytical solution of the integral is known. We choose the case $f(\tau) = \sin(\tau)$ where the history integral can be computed with the help of the Anger function $J_\nu(t)$ [24], which is a generalization of the Bessel function $J_n(t)$ to fractional values of n ,

$$\int_0^t \frac{\sin(\tau)}{\sqrt{t-\tau}} d\tau = \frac{1}{2}\pi\sqrt{t} \left(J_{\frac{1}{2}}(t) - J_{-\frac{1}{2}}(t) \right) \equiv I(t). \quad (12)$$

To verify the order of the scheme let us analyze the global error

$$\varepsilon(h) = \max_{t \in [0,10]} |I(t) - I_{\text{num}}(t, h)|,$$

where $I(t)$ denotes the exact value of the integral in (12) and $I_{\text{num}}(t, h)$ the numerically approximated value. Fig. 1 shows the dependence of this global error on h for the three numerical quadrature schemes given here (specified by α_j^n , β_j^n , γ_j^n) and a second order, semi-open Newton-Cotes scheme [25]. We see that errors of the schemes are proportional to h^{m+1} for the m -th order scheme, thus verifying the order of the quadrature schemes (at least for this test-case). Also we see that a standard second order quadrature scheme (the

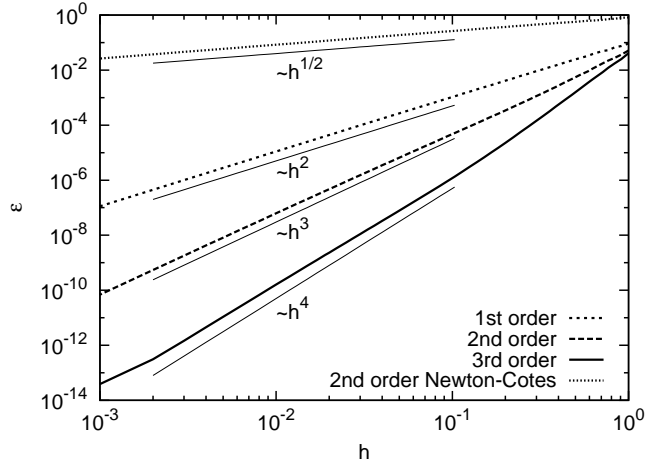


Figure 1: Scaling of the global error $\varepsilon(h)$ of the quadrature schemes for the test-case $f(\tau) = \sin(\tau)$.

Newton-Cotes scheme) performs very badly as the error scales only with \sqrt{h} . This is also true for higher order Newton-Cotes schemes and is due to the necessity of a numerical evaluation of the kernel near the singularity.

The correctness of the quadrature schemes has also been tested using the analytically treatable case of a polynomial of arbitrary order and led to similar results.

3. Integration of the full Maxey-Riley equation

In this section the quadrature scheme developed in the previous section will be incorporated in a multi-step integration scheme for the full Maxey-Riley equation. To this end we formulate the Maxey-Riley equation for the velocity difference $\mathbf{w} = \mathbf{v} - \mathbf{u}$ in a given flow field \mathbf{u} :

$$\frac{d\mathbf{w}}{dt} = (R-1) \frac{d\mathbf{u}}{dt} - R\mathbf{w} \cdot \nabla \mathbf{u} - \frac{R}{S} \mathbf{w} - R\sqrt{\frac{3}{\pi S}} \frac{d}{dt} \int_{t_0}^t K(t-\tau) \mathbf{w}(\tau) d\tau. \quad (13)$$

Together with the evolution equation for the particle position

$$\frac{d\mathbf{r}}{dt} = \mathbf{v} = \mathbf{w} + \mathbf{u}$$

equation (13) fully specifies the motion of an inertial particle in a fluid. Integrating (13) from t to $t+h$ and using the abbreviations

$$\begin{aligned} \mathbf{G} &= (R-1) \frac{d\mathbf{u}}{dt} - R\mathbf{w} \cdot \nabla \mathbf{u} - \frac{R}{S} \mathbf{w} \\ \mathbf{H} &= -R\sqrt{\frac{3}{\pi S}} \int_{t_0}^t K(t-\tau) \mathbf{w}(\tau) d\tau \end{aligned}$$

we obtain

$$\mathbf{w}(t+h) = \mathbf{w}(t) + \int_t^{t+h} \mathbf{G}(\tau) d\tau + \mathbf{H}(t+h) - \mathbf{H}(t). \quad (14)$$

Here the integration of the history term can be performed trivially due to relation (4). This simplifies the integration scheme considerably. Furthermore, we now have to compute a history integral of \mathbf{w} and not $d\mathbf{w}/d\tau$, where the former will generally fluctuate less and is therefore better suited for a numerical

quadrature. The history integral \mathbf{H} can be computed with the schemes developed in section 2. The integral of \mathbf{G} can be approximated using polynomial interpolation. We use only the present and previous values of \mathbf{G} for this approximation in order to obtain an explicit scheme:

$$\begin{aligned}\int_t^{t+h} \mathbf{G}(\tau) d\tau &= h\mathbf{G}(t) + \mathcal{O}(h^2) \\ \int_t^{t+h} \mathbf{G}(\tau) d\tau &= \frac{h}{2} (3\mathbf{G}(t) - \mathbf{G}(t-h)) + \mathcal{O}(h^3) \\ \int_t^{t+h} \mathbf{G}(\tau) d\tau &= \frac{h}{12} (23\mathbf{G}(t) - 16\mathbf{G}(t-h) + 5\mathbf{G}(t-2h)) + \mathcal{O}(h^4).\end{aligned}$$

These expressions can be found in any literature on Adams-Bashforth multi-step methods, e.g. [25].

A final point which we have to consider before writing down the complete scheme, is that

$$\mathbf{H}(t+h) = \sum_{j=0}^{n+1} \mu_j^{n+1} \mathbf{w}(\tau_{n+1-j}) + \mathcal{O}(h^m)$$

depends on $\mathbf{w}(\tau_{n+1}) = \mathbf{w}(t+h)$ and thus can not be evaluated before $\mathbf{w}(t+h)$ is known. This is due to the implicitness of the Maxey-Riley equation. However this is easily dealt with by bringing $\mathbf{w}(t+h)$ to the left-hand side of (14).

If we now consider (14) on the grid $t_n = t_0 + nh$, define $\xi = R\sqrt{3/(\pi S)}\sqrt{h}$ and use abbreviations of the type $\mathbf{w}_n = \mathbf{w}(t_n)$ we can specify the complete integration schemes of first, second and third order for the Maxey-Riley equation:

$$\begin{aligned}\mathbf{r}_{n+1} &= \mathbf{r}_n + h(\mathbf{w}_n + \mathbf{u}_n) + \mathcal{O}(h^2), \\ (1 + \xi\alpha_0^{n+1}) \mathbf{w}_{n+1} &= \mathbf{w}_n + h\mathbf{G}_n - \xi \sum_{j=0}^n (\alpha_{j+1}^{n+1} \mathbf{w}_{n-j} - \alpha_j^n \mathbf{w}_{n-j}) + \sqrt{t_n - t_0} \mathcal{O}(h^2),\end{aligned}\tag{15}$$

$$\begin{aligned}\mathbf{r}_{n+1} &= \mathbf{r}_n + \frac{h}{2} (3(\mathbf{w}_n + \mathbf{u}_n) - (\mathbf{w}_{n-1} + \mathbf{u}_{n-1})) + \mathcal{O}(h^3), \\ (1 + \xi\beta_0^{n+1}) \mathbf{w}_{n+1} &= \mathbf{w}_n + \frac{h}{2} (3\mathbf{G}_n - \mathbf{G}_{n-1}) - \xi \sum_{j=0}^n (\beta_{j+1}^{n+1} \mathbf{w}_{n-j} - \beta_j^n \mathbf{w}_{n-j}) + \sqrt{t_n - t_0} \mathcal{O}(h^3),\end{aligned}\tag{16}$$

$$\begin{aligned}\mathbf{r}_{n+1} &= \mathbf{r}_n + \frac{h}{12} (23(\mathbf{w}_n + \mathbf{u}_n) - 16(\mathbf{w}_{n-1} + \mathbf{u}_{n-1}) + 5(\mathbf{w}_{n-2} + \mathbf{u}_{n-2})) + \mathcal{O}(h^4), \\ (1 + \xi\gamma_0^{n+1}) \mathbf{w}_{n+1} &= \mathbf{w}_n + \frac{h}{12} (23\mathbf{G}_n - 16\mathbf{G}_{n-1} + 5\mathbf{G}_{n-2}) - \xi \sum_{j=0}^n (\gamma_{j+1}^{n+1} \mathbf{w}_{n-j} - \gamma_j^n \mathbf{w}_{n-j}) + \sqrt{t_n - t_0} \mathcal{O}(h^4).\end{aligned}\tag{17}$$

The coefficients α_j^n , β_j^n and γ_j^n are given in section 2. One reason to include the first and second order schemes here (besides the third order one) is that one cannot start the integration with the third order scheme as the previous values \mathbf{G}_{n-1} , \mathbf{G}_{n-2} are not available at the beginning. This is a problem common to all multi-step methods. The simplest solution is to use the first and second order schemes for the first two steps and the third order scheme for the rest. To perform the first step of the integration ($n=0$) with (15) the coefficients α_j^0 are needed, which we define to be zero as no history is present at $t=t_0$. Ideally, we would perform the second step ($n=1$) with (16). But β_j^n is defined only for $n \geq 2$, leaving us with two options: (i) perform the second step with the first order scheme or (ii) define $\beta_j^1 \equiv \alpha_j^1$ and accept a reduced accuracy. The second option is at least as accurate as the first one and will thus be assumed in the

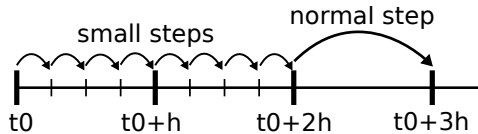


Figure 2: Procedure to start the integration with multi-step methods.

following. The same considerations are applicable to the third order scheme (17), leading to the definition $\gamma_j^2 \equiv \beta_j^2$ and allowing its use for $n \geq 2$ (instead of for $n \geq 3$).

The integration methods (15)-(17) can be viewed as an extension of the Adams-Bashforth multi-step methods to the case of an integro-differential equation with memory. In its present form the quadrature schemes in section 2 are best suited for multi-step methods with a fixed time-step. In other schemes, for example Runge-Kutta, half-steps are necessary, but they cannot be evaluated with the current formulation of the quadrature schemes. Furthermore, multi-step methods allow to profit from the fact that an integral of the history force can be computed by simply dropping a derivative (see (14) and comments below).

3.1. Comments on the Implementation

Using lower order schemes for the first two steps makes them less accurate. A more advanced strategy is to begin the integration with a smaller time-step to account for the reduced accuracy and switch on the third order scheme with the normal time-step when it is applicable. This procedure is demonstrated in figure 2: At the beginning of the integration, eight small steps with time-step $h' = h/4$ are taken. From the time-point $t_0 + 2h$ on the third order scheme can be applied with the normal step size h as enough previous values are available then. In practice the size h' of the small steps can be much smaller than h , e.g. $h' = h/100$. This procedure can be further refined, e.g. in figure 2 it would be sufficient to take steps of $h/2$ in the interval $[t_0 + h, t_0 + 2h]$. However, the savings in computational time due to this optimization will generally be not large enough to compensate for the increased complexity of the algorithm.

Because of the dependency of the coefficients α_j^n , β_j^n and γ_j^n on n one might be tempted to recompute them for every time-step n . This would make the schemes quite slow. Fortunately the coefficients can be precomputed and stored efficiently, because they depend on n only for the last few j . We will exemplify this for α_j^n given in (9); the generalization to the higher order coefficients β_j^n and γ_j^n is straightforward. As α_j^n depends on n only when $j = n$, we can express it as

$$\alpha_j^n = \begin{cases} a_j & j < n \\ b_n & j = n \end{cases} \quad \text{with} \quad a_j = \frac{4}{3} \begin{cases} 1 & j = 0 \\ (j-1)^{3/2} + (j+1)^{3/2} - 2j^{3/2} & j > 0 \end{cases}$$

and $b_n = \frac{4}{3} \left((n-1)^{3/2} - n^{3/2} + \frac{6}{4}\sqrt{n} \right)$. Let now N be the maximal number of time-steps we wish to perform. We then can precompute a_j and b_n for $j, n \leq N$ once and easily construct α_j^n from them for every $n \leq N$. This is particularly beneficial when one wants to integrate a large number of particle trajectories. As the coefficients α_j^n , β_j^n and γ_j^n contain differences of large numbers (for large j), they should be precomputed with a high numerical precision. For the examples shown here they have been computed with quad precision (i.e. 128-bit floating point number) and stored with double precision.

3.2. Testing the Accuracy of the Schemes

To test the accuracy of the whole integration scheme, the motion of a particle in the flow $\mathbf{u}(\mathbf{r}) = |\mathbf{r}| \mathbf{e}_\varphi$ (rigid body rotation) will be considered. Fortunately, in this case there is an analytical solution for the full Maxey-Riley equation found by Candelier et al. [12]. Qualitatively, the solution is a spiraling motion outwards or inwards depending on whether the density of the particle is larger or smaller than that of the fluid, i.e. $R < 1$ or $R > 1$. Asymptotically the distance of the particle from the center grows exponentially, $|\mathbf{r}(t)| \sim \exp(\lambda t)$. The ejection rate λ depends on the presence of the history force and thus the trajectories of particles with memory and without memory deviate rather quickly. This makes this flow a good choice

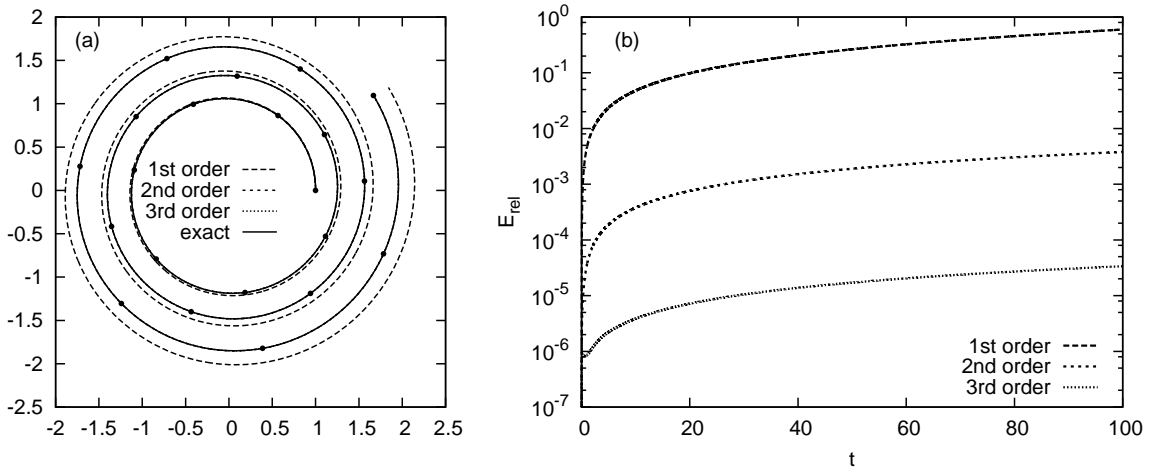


Figure 3: (a) The exact trajectory of a particle starting at $\mathbf{r}_0 = (1, 0)$ with $\mathbf{w}_0 = \mathbf{0}$ and the parameters $R = 0.75$ and $S = 0.3$. The dots show the position at integer time units. Also shown are the approximations of first, second and third order for $h = 10^{-2}$, where the latter two are overlapped by the exact trajectory and are thus not visible. (b) The relative error of the numerical solutions obtained by the first, second and third order schemes (15)-(17) with $h = 10^{-2}$.

for a test of the integration scheme as an inaccurate computation of the history force is expected to lead to strong deviations from the analytically known trajectories.

Figure 3a shows the exact solution together with the numerical solutions of first, second and third order obtained by (15)-(17) with $h = 10^{-2}$. Only the the first order approximation is visible, whereas the second and third order ones are overlapped by the exact trajectory. To understand this let us examine the relative error

$$E_{\text{rel}}(t, h) = \frac{|\mathbf{r}(t) - \mathbf{r}_{\text{num}}(t, h)|}{|\mathbf{r}(t)|},$$

where $\mathbf{r}_{\text{num}}(t, h)$ is the numerical and $\mathbf{r}(t)$ the exact solution. Figure 3b shows this quantity for $h = 10^{-2}$. We see that the error improves by approximately two orders of magnitude for each additional order of the scheme, thus explaining the overlapping of the second and third order approximations by the exact solution in figure 3a. Figure 3b also gives information about the quality of the approximation as a function of time. For example, at $t = 100$ the first order approximation has a very large error of ca. 60%, whereas the second and third order approximations are rather accurate with errors of ca. 0.4% and 0.003%. At $t = 100$ the distance of the particle from the center is $|\mathbf{r}(100)| \approx 31$ whereas for a particle without memory (i.e. when the history force is neglected) it is ≈ 476 , showing that the history force has a strong influence on the particle's motion. Therefore an accurate computation of the history force is essential for a high precision approximation, as obtained by the second and third order schemes.

To examine the dependence of the error on the width of the time-step let us again use the global error

$$\varepsilon(h) = \max_{t \in [0, 100]} |\mathbf{r}(t) - \mathbf{r}_{\text{num}}(t, h)|,$$

where $\mathbf{r}_{\text{num}}(t, h)$ is the numerical and $\mathbf{r}(t)$ the exact solution. Figure 4 shows that the error of the m -th order scheme scales as h^m . The global error is expected to be proportional to the number of time-steps, i.e. for a one-step error of $\mathcal{O}(h^{m+1})$ we expect the global error to behave as $t_{\text{max}}/h \mathcal{O}(h^{m+1}) = \mathcal{O}(h^m)$, where t_{max} is the integration length. Thus the benchmark shown in Figure 4 confirms the order of the schemes.

From the dependence of ε on h we can see that rather small global errors are achievable with moderately small time-steps when the second or third order scheme is used. Let us exemplify the importance of the higher order schemes for the computational costs with the measurements shown in Figure 4. Suppose we would like to achieve a maximal global error of $\varepsilon = 1$, which corresponds to a relative error of approximately $\varepsilon/|\mathbf{r}(100)| \approx 3\%$. Then we would have to choose at least $h_1 \approx 8 \cdot 10^{-4}$, $h_2 \approx 3 \cdot 10^{-2}$ and $h_3 \approx 10^{-1}$ for the

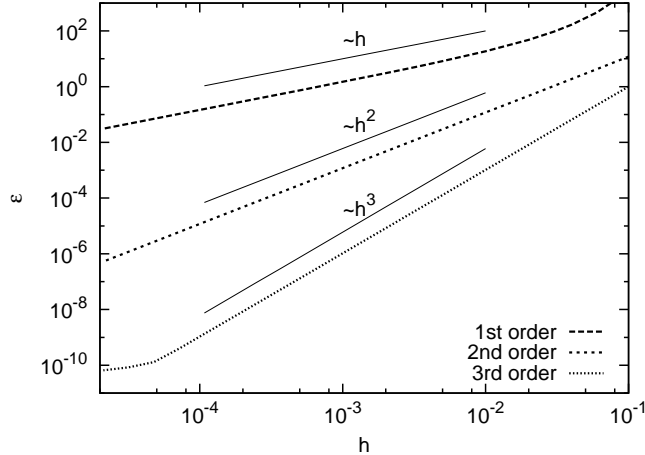


Figure 4: Scaling of the global error $\varepsilon(h)$ as a function of the time-step h . The parameters of the particle are $R = 0.75$ and $S = 0.3$; it started at $\mathbf{r}_0 = (1, 0)$ with $\mathbf{w}_0 = \mathbf{0}$.

first, second and third order scheme (see Figure 4). This would lead to $N_1 = 100/h_1 \approx 10^5$, $N_2 \approx 3 \cdot 10^3$ and $N_3 \approx 10^3$ necessary time-steps for the three schemes. The reduction in the number of time-steps is considerable. However the reduction in the computational costs are even more dramatic as they are proportional to N^2 , e.g. using the third order scheme would reduce the computational cost roughly by a factor of $N_1^2/N_3^2 \approx 10^4$ compared to the first order scheme. This ratio would become even higher when we go to smaller error bounds. It should be emphasized here that all three integration schemes have basically the same computational cost per time-step. This is because the history force is computed by a weighted sum in all three cases (8),(10),(11) and the coefficients can be precomputed as discussed above.

4. Stability of the Integration Scheme

An important property of numerical algorithms is stability, i.e. errors remain bounded during the iteration of the algorithm. For ordinary differential equations numerical stability is usually determined by applying the integration scheme to the equation

$$\frac{dw}{dt} = -kw, \quad (18)$$

and verifying whether the numerical solution converges to zero. To check the stability of our schemes we use the equation

$$\frac{dw}{dt} = -k \left(w + \frac{d}{dt} \int_{t_0}^t \frac{w(\tau)}{\sqrt{t-\tau}} d\tau \right), \quad (19)$$

which is the Maxey-Riley equation (5) in still fluid ($u = 0$) with $R = \pi k/3$ and $S = \pi/3$. The solution of this equation converges to zero algebraically ($\sim t^{-1.5}$) in contrast to an exponential convergence for (18). In general k is a complex number. However, here the analysis is restricted to purely real and positive values of k . In this case, k can be set to 1 by rescaling the time and we can analyze stability as a function of the time-step h only.

Applying the integration schemes (15)-(17) to the test equation (19) yields in each case a recurrence relation for w_n . A recurrence relation (and thus the corresponding numerical scheme) is said to be stable when $\lim_{n \rightarrow \infty} w_n = 0$ for every initial condition. Without the history force w_n depends only on a few previous values, e.g. w_{n-1} , w_{n-2} and w_{n-3} for (17). In this case the stability can be checked analytically. However with the history force, w_n depends on all previous values and we can no longer analytically determine

	order of the scheme		
	1	2	3
with memory	4.7627	0.9428	0.3886
without memory	2.0000	1.0000	0.5455

Table 1: Stability thresholds h_{th} of the numerical schemes (15)-(17) compared with those without the history force in (19).

the stability region. Therefore we turn to a numerical stability analysis: the scheme is iterated for 10^6 time-steps and it is checked whether w_n converges to zero. This procedure has been carried out for a large number of different values of the time-step h and it has been found that w_n either converged to zero or became infinite. These two regimes are separated by the stability threshold h_{th} , i.e. for $h < h_{\text{th}}$ the iterated scheme converges to zero and is thus stable and for $h > h_{\text{th}}$ the iterated scheme diverges and is thus unstable. Table 1 shows the stability thresholds for the first, second and third order schemes (15)-(17). For comparison the row “without memory” contains the stability thresholds of the schemes without the history force, i.e. normal Adams-Bashforth schemes⁷. For the first order method the inclusion of the history force increases the stability threshold, i.e. the scheme becomes more stable. In the case of the second and third order schemes the inverse is true; the stability threshold is slightly lower and the schemes are less stable when memory is included. However the influence of the history force on the stability of the schemes seems to be rather weak as the stability thresholds vary only by a factor of order unity. Summing up, one can say that the integration schemes (15)-(17) seem to have very similar stability properties as the corresponding Adams-Bashforth methods for ordinary differential equations.

5. Discussion and Conclusion

In this paper we developed a systematic way for the derivation of higher order numerical integration schemes for the full Maxey-Riley equation, including the history force. Due to the singularity of the integrand of the history force a special numerical scheme is needed. Explicit specifications of the numerical schemes of first, second and third order with an accuracy of $\mathcal{O}(h^2)$, $\mathcal{O}(h^3)$ and $\mathcal{O}(h^4)$, respectively, have been given. Furthermore the correctness and the order of the schemes have been verified by comparison with known analytical solutions.

The accuracy of the second and third order schemes represents a substantial improvement compared with the methods available in the literature. As discussed above the computational cost per time-step does not depend on the order of the scheme. Thus, by using these schemes one gets the additional accuracy or, alternatively, the reduced number of time-steps essentially for free.

As mentioned in the introduction, different forms of the history force have been proposed for the case of finite particle Reynolds numbers $Re = a|\mathbf{v} - \mathbf{u}|/\nu$. In [17, 18] the modified history force is based on a kernel proposed by Mei, which decays faster than the Basset kernel for large time lags. This kernel can be expressed as follows (in dimensionless units and to be used in (2))

$$K_{\text{Mei}} = \frac{1}{\sqrt{t-\tau}} \left\{ 1 + \left[\sqrt{\frac{\pi(t-\tau)^3}{St^3}} \frac{Re^3}{16(0.75 + c_2 Re)^3} \right]^{1/c_1} \right\}^{-c_1}. \quad (20)$$

The parameters c_1 and c_2 have been empirically determined in [17] as $c_1 = 2$, $c_2 = 0.105$ and in [18] as $c_1 = 2.5$, $c_2 = 0.2$. Note that in (20) the Basset kernel $1/\sqrt{t-\tau}$ appears as a factor; in particular it is the only factor with a divergent behavior. Thus we can use the methods specified in section 3 to numerically evaluate this form of the history force by pulling the second factor in (20) into $f(\tau)$,

$$f(\tau) = \left(\frac{d\mathbf{v}}{d\tau} - \frac{d\mathbf{u}}{d\tau} \right) \left\{ 1 + \left[\sqrt{\frac{\pi(t-\tau)^3}{St^3}} \frac{Re^3}{16(0.75 + c_2 Re)^3} \right]^{1/c_1} \right\}^{-c_1},$$

⁷The computed thresholds without memory are consistent with the known stability regions of the Adams-Bashforth methods.

and use the quadrature schemes (8), (10) and (11). Note that we can not make use of the relation (4) as the above expression for f can not be explicitly formulated as a derivative of some function. Thus the schemes (15)-(17) have to be modified for the use with this kernel (essentially the history force has to become part of \mathbf{G} in section 3).

Lovalenti and Brady [16] derived a history force of the form

$$\int_{-\infty}^t \frac{1}{(t-\tau)^{3/2}} g(t, \tau, \mathbf{v}, \mathbf{u}) d\tau = \int_{-\infty}^t \frac{2}{\sqrt{t-\tau}} \frac{dg}{d\tau} d\tau \quad (21)$$

where $g(t, \tau, \mathbf{v}, \mathbf{u})$ has a complicated dependence on the particle and fluid velocity. In the limit $\tau \rightarrow t$ one finds $g \sim t - \tau$; thus the left integral in (21) is well defined and the identity (21) holds. The right integral in (21) again contains the Basset kernel. Furthermore the function $\frac{dg}{d\tau}$ has no singularities, we therefore can use the coefficients from section 3 for a numerical evaluation of the history force, by choosing $f = 2\frac{dg}{d\tau}$. Thus the numerical schemes presented here can be used with the standard Basset history force as well as with other proposed forms of the history force.

There are several reasons limiting the wide use of the history force in simulations of inertial particles. On the one hand there is some disagreement on the particular form of the history force in the case of finite particle Reynolds numbers. On the other hand there are computational problems: the high numerical costs and the absence of high accuracy schemes. As has been shown, the later two points can be effectively addressed with the higher order schemes developed here. I hope that this will resolve some of the hurdles in the research on the history force and facilitate investigations of its role in the motion of inertial particles.

Acknowledgment

I would like to thank Tamás Tél and Michael Wilczek for very helpful discussions.

Appendix A. Details on the derivation of the quadrature scheme

In section 2 the derivation of the quadrature scheme was presented in a simplified, not fully detailed way. This appendix will present the technical details and give a complete, but somewhat laborious derivation.

To interpolate $f(\tau)$ in the interval $[\tau_i, \tau_{i+1}]$, Lagrangian polynomial interpolation is used:

$$f(\tau) = \sum_{k=0}^m f(\theta_{ik}^{nm}) L_{ik}^{nm}(\tau) + \mathcal{O}(h^{m+1}) \quad L_{ik}^{nm}(\tau) = \prod_{\substack{l=0 \\ l \neq k}}^m \frac{\tau - \theta_{il}^{nm}}{\theta_{ik}^{nm} - \theta_{il}^{nm}}.$$

Here the full dependence of the time-points θ_{ik}^{nm} on n and m has been written out explicitly. In section 2 we have chosen $\theta_{ik}^{nm} = \tau_{i-\lfloor m/2 \rfloor + k}$. Thus the dependence on m and i is obvious, and we will see in a moment why a dependence on n is necessary. The problem with the above definition of θ_{ik}^{nm} is that for $i < \lfloor m/2 \rfloor$ we would obtain time-points outside the integration interval $[t_0, t]$, e.g. $\theta_{0,0}^{nm} = \tau_{-\lfloor m/2 \rfloor} = t_0 - \lfloor m/2 \rfloor h$, and thus would have to rely on values of $f(\tau)$ that are not available. A similar problem occurs for $i > n - m + \lfloor m/2 \rfloor$. To solve this, we need a definition of θ_{ik}^{nm} that deals with the special cases $i < \lfloor m/2 \rfloor$ and $i > n - m + \lfloor m/2 \rfloor$. For this let us define the offset o_i^{nm} as

$$o_i^{nm} = \begin{cases} 0 & 0 \leq i \leq \lfloor m/2 \rfloor \\ i - \lfloor m/2 \rfloor & \lfloor m/2 \rfloor < i < n - m + \lfloor m/2 \rfloor \\ n - m & n - m + \lfloor m/2 \rfloor \leq i \leq n - 1 \end{cases}$$

and $\theta_{ik}^{nm} = \tau_{o_i^{nm} + k}$. The offset is defined so that it is equal to $i - \lfloor m/2 \rfloor$ (corresponding to our naive ansatz $\theta_{ik}^{nm} = \tau_{i-\lfloor m/2 \rfloor + k}$) where possible and is set to 0 and $n - m$ where we would obtain time-points outside the integration interval $[t_0, t]$.

The interpolating polynomial for $f(\tau)$ in the interval $[\tau_i, \tau_{i+1}]$ can now be expressed as

$$f(\tau) = \sum_{k=0}^m f(\tau_{o_i^{nm}+k}) L_{ik}^{nm}(\tau) + \mathcal{O}(h^{m+1}) \quad L_{ik}^{nm}(\tau) = \prod_{\substack{l=0 \\ l \neq k}}^m \frac{\tau - \tau_{o_{ik}^{nm}+l}}{\tau_{o_{ik}^{nm}+k} - \tau_{o_{ik}^{nm}+l}}$$

and integrated to yield

$$\int_{t_0}^t d\tau K(t-\tau) f(\tau) = \sum_{i=0}^{n-1} \sum_{k=0}^m f(\tau_{o_i^{nm}+k}) \underbrace{\int_{\tau_i}^{\tau_{i+1}} d\tau K(t-\tau) L_{ik}^{nm}(\tau)}_{\lambda_{ik}^{nm}} + E = \sum_{i=0}^{n-1} \sum_{k=0}^m f(\tau_{o_i^{nm}+k}) \lambda_{ik}^{nm} + E, \quad (\text{A.1})$$

where $E = \int_{t_0}^t K(t-\tau) d\tau \mathcal{O}(h^{m+1})$ is the error term.

Let us now reorder the double sum to a single sum of the type $\sum_j \mu_j^{nm} f(\tau_{n-j})$. As already mentioned in section 2, it turns out as beneficial to index the coefficients μ_j^{nm} in reversed order, i.e. μ_0^{nm} and μ_n^{nm} correspond to $f(\tau_n)$ and $f(\tau_0)$ respectively. For the following calculations we will use the theta function, which is defined here in the following way: Θ takes logical conditions as arguments and has the value 1 if the condition is satisfied and 0 otherwise, e.g. $\Theta(i < 0)$ is equal to 1 when $i < 0$. The double sum in (A.1) can be expressed as a single sum

$$\sum_{i=0}^{n-1} \sum_{k=0}^m f(\tau_{o_i^{nm}+k}) \lambda_{ik}^{nm} = \sum_{j=0}^n f(\tau_{n-j}) \sum_{i,k} \Theta(o_i^{nm} + k = n - j) \lambda_{ik}^{nm} = \sum_{j=0}^n \mu_j^{nm} f(\tau_{n-j}),$$

with the coefficients

$$\mu_j^{nm} = \sum_{i=0}^{n-1} \sum_{k=0}^m \Theta(o_i^{nm} + k = n - j) \lambda_{ik}^{nm}.$$

Using the definition of o_i^{nm} , the sum over i can be split into three terms (for the purpose of a compact presentation the indices n and m will be omitted and the abbreviations $a = \lfloor m/2 \rfloor$ and $b = m - \lfloor m/2 \rfloor$ will be used):

$$\mu_j = \sum_{i=0}^{a-1} \sum_{k=0}^m \Theta(k = n - j) \lambda_{ik} + \sum_{i=a}^{n-b} \sum_{k=0}^m \Theta(i - a + k = n - j) \lambda_{ik} + \sum_{i=n-b+1}^{n-1} \sum_{k=0}^m \Theta(n - m + k = n - j) \lambda_{ik}.$$

The conditions in the theta functions can be used to get rid of one summation. For example in the first term the condition $k = n - j$ is satisfied at most for one value of k and thus k can be replaced by $n - j$. However one has to keep in mind that the condition may be not satisfiable at all (it is satisfiable when $0 \leq n - j \leq m$). Applying this kind of reasoning to the other two terms yields

$$\begin{aligned} \mu_j = \Theta(0 \leq n - j \leq m) \sum_{i=0}^{a-1} \lambda_{i,n-j} + \sum_{k=0}^m \Theta(a \leq n - j - k + a \leq n - b) \lambda_{n-j-k+a,k} \\ + \Theta(0 \leq m - j \leq m) \sum_{i=n-b+1}^{n-1} \lambda_{i,m-j}. \end{aligned}$$

In the second term the summation over i (instead of k) has been removed. The satisfiability condition depends on k and thus has to remain inside the sum. Simplifying the conditions we obtain

$$\mu_j = \Theta(n - m \leq j \leq n) \sum_{i=0}^{a-1} \lambda_{i,n-j} + \sum_{k=0}^m \Theta(m - j \leq k \leq n - j) \lambda_{n-j-k+a,k} + \Theta(0 \leq j \leq m) \sum_{i=n-b+1}^{n-1} \lambda_{i,m-j}.$$

The condition in the second term can be used to narrow the summation range, and we obtain the final expression for the coefficients μ_j^{nm}

$$\mu_j^{nm} = \Theta(n-m \leq j \leq n) \sum_{i=0}^{a-1} \lambda_{i,n-j}^{nm} + \sum_{k=\max(0,m-j)}^{\min(m,n-j)} \lambda_{n-j-k+a,k}^{nm} + \Theta(0 \leq j \leq m) \sum_{i=n-b+1}^{n-1} \lambda_{i,m-j}^{nm}.$$

For the case of the standard kernel (3) the integrals λ_{ik}^{nm} can be computed analytically and thus the coefficients μ_j^{nm} . This has been done by means of the computer algebra system Maple and the resulting expressions for the coefficients are given in section 2.

References

- [1] C. Crowe, J. Schwarzkopf, M. Sommerfeld, Y. Tsuji, *Multiphase flows with droplets and particles*, CRC press, 2011.
- [2] G. Falkovich, A. Fouxon, M. Stepanov, Acceleration of rain initiation by cloud turbulence, *Nature* 419 (6903) (2002) 151–154.
- [3] A. Bracco, P. H. Chavanis, A. Provenzale, E. A. Spiegel, Particle aggregation in a turbulent keplerian flow, *Physics of Fluids* 11 (8) (1999) 2280–2287.
- [4] J. C. Zahnow, R. D. Vilela, U. Feudel, T. Tél, Aggregation and fragmentation dynamics of inertial particles in chaotic flows, *Phys. Rev. E* 77 (2008) 055301.
- [5] I. Benczik, Z. Toroczka, T. Tél, Selective sensitivity of open chaotic flows on inertial tracer advection: Catching particles with a stick, *Phys. Rev. Lett.* 89 (16) (2002) 164501.
- [6] W. Tang, G. Haller, J.-J. Baik, Y.-H. Ryu, Locating an atmospheric contamination source using slow manifolds, *Phys. Fluids* 21 (4) (2009) 043302.
- [7] T. Sapsis, G. Haller, Inertial particle dynamics in a hurricane, *J. Atmos. Sci.* 66 (8) (2009) 2481–2492.
- [8] T. Sapsis, J. Peng, G. Haller, Instabilities on prey dynamics in jellyfish feeding, *Bull. Math. Biol.* 73 (8) (2011) 1841–1856.
- [9] M. R. Maxey, J. J. Riley, Equation of motion for a small rigid sphere in a nonuniform flow, *Phys. Fluids* 26 (4) (1983) 883–889.
- [10] T. R. Auton, J. C. R. Hunt, M. Prud’Homme, The force exerted on a body in inviscid unsteady non-uniform rotational flow, *J. Fluid Mech.* 197 (1988) 241–257.
- [11] N. Mordant, J. Pinton, Velocity measurement of a settling sphere, *Eur. Phys. J. B* 18 (2) (2000) 343–352.
- [12] F. Candelier, J. R. Angilella, M. Souhar, On the effect of the Boussinesq–Basset force on the radial migration of a Stokes particle in a vortex, *Physics of Fluids* 16 (5) (2004) 1765–1776.
- [13] V. Armenio, V. Fiorotto, The importance of forces acting on particles in turbulent flows, *Phys. Fluids* 13 (2001) 24372440.
- [14] M. van Aartrijk, H. J. H. Clercx, Vertical dispersion of light inertial particles in stably stratified turbulence: The influence of the Basset force, *Physics of Fluids* 22 (1) (2010) 013301.
- [15] A. Daitche, T. Tél, Memory effects are relevant for chaotic advection of inertial particles, *Phys. Rev. Lett.* 107 (2011) 244501.
- [16] P. M. Lovalenti, J. F. Brady, The hydrodynamic force on a rigid particle undergoing arbitrary time-dependent motion at small Reynolds number, *J. Fluid Mech.* 256 (1993) 561–605.
- [17] R. Mei, Flow due to an oscillating sphere and an expression for unsteady drag on the sphere at finite Reynolds number, *Journal of Fluid Mechanics* 270 (1994) 133–174.
- [18] A. Dorgan, E. Loth, Efficient calculation of the history force at finite Reynolds numbers, *Int. J. Multiphase Flows* 33 (2007) 833–848.
- [19] E. Loth, A. Dorgan, An equation of motion for particles of finite Reynolds number and size, *Environmental Fluid Mechanics* 9 (2) (2009) 187–206.
- [20] E. E. Michaelides, A novel way of computing the Basset term in unsteady multiphase flow computations, *Phys. Fluids A* 4 (1992) 1579–1582.
- [21] F. Bombardelli, A. González, Y. Niño, et al., Computation of the particle Basset force with a fractional-derivative approach, *Journal of Hydraulic Engineering* 134 (2008) 1513.
- [22] M. van Hinsberg, J. ten Thije Boonkamp, H. Clercx, An efficient, second order method for the approximation of the Basset history force, *J. Comput. Phys.* 230 (2011) 1465–1478.
- [23] M. R. Maxey, The equation of motion for a small rigid sphere in a nonuniform or unsteady flow, *Gas–Solid Flows*, ASME/FED 166 (1993) 57–62.
- [24] M. Abramowitz, I. Stegun, *Handbook of Mathematical Functions*, 1972.
- [25] W. Press, B. Flannery, S. Teukolsky, W. Vetterling, P. Kramer, *Numerical recipes: the art of scientific computing*, Cambridge University Press, 1987.